What are the drivers of riparian vegetation recruitment and establishment in an alpine embanked river?

Authors: J. Godfroy[1*]; L. Borgniet[1]; T. Boissy[2]; H. Piégay[3]; G. Melun[4]; P. Janssen[1].

[1] Univ. Grenoble Alpes, INRAE, LESSEM, St-Martin d'Hères, France

[2] Syndicat Mixte de l'Isère et de l'Arc en Combe de Savoie, Albertville, France

[3] Univ. of Lyon, ENS Lyon, CNRS, UMR 5600 EVS, Lyon, France

[4] Office Français de la Biodiversité (OFB), Direction de la recherche et de l'appui scientifique, Vincennes, France

* corresponding author : julien.godfroy@inrae.fr

Abstract

1 – Rejuvenation operations are often conducted in rivers to manage vegetation encroachment and balance biodiversity benefits and flood risks. Understanding the drivers of vegetation recruitment and establishment is necessary to implement these operations but requires monitoring at spatial and temporal scales that are suited to pioneer riparian environment.

2 – Bi-yearly drone surveys were used to retrieve the trajectory of pioneer vegetation in a six kilometres reach of the Isère River (France) following rejuvenation operations. Visible images acquired at the beginning and the end of six consecutive vegetation periods were classified using a convolutional neural network and changes in vegetation cover through time were characterized using spatial operations across dates.

3 – Vegetation encroachment in the reach was driven by patch expansion and presented a high inter-annual variability. Provided environmental conditions were favourable, vegetation could cover 20% of bar surfaces in a two-year period following rejuvenation actions. Vegetation destruction in the reach was on the other hand mainly driven by vegetation clearing operations.

4 – Vegetation recruitment was found to be mainly driven by the hydrological conditions during the seed dispersal and germination period in May and June. Prolonged bar submersion for flow levels starting at 125 $m^3.s^{-1}$ led to lower recruitment while prolonged dry periods were instead favourable to vegetation encroachment. Under favourable hydrological conditions, recruitment mainly occurred in areas that were covered by fine sediments or water at the beginning of the vegetative period.

5 – Spring and winter floods did not result in significant vegetation destruction when plants had a least a year to establish. The surfaces of vegetation destroyed by the Isère River was always lower than the net gain in vegetation cover for each period, and the only spike in vegetation destruction occurred when most vegetation in the reach was less than one year old.

6 – Synthesis: Summer hydrology played a key role in vegetation encroachment in the reach by providing either favourable (*i.e.*, prolonged dry periods and no high flows late June) or unfavourable conditions for vegetation recruitment and establishment. Timing eco-morphogenic releases to sustain submersion could help prevent encroachment.

Keywords.

46 Anthropized rivers; Pioneer riparian vegetation; Recruitment processes; Remote Sensing;
47 Biogeomorphology; Ecohydrology

1. Introduction.

River functioning has been altered worldwide by a wide range of pressures such as land use change, damming, and channelization (Belletti et al., 2020; Entwistle et al., 2019; Grill et al., 2019). By modifying the flow and sediment regimes of rivers, human activities have resulted in widespread changes in river geomorphology (Liébault and Piégay, 2002; Surian and Rinaldi, 2003), with impacts on riparian zones and related plants communities (Corenblit et al., 2007; Gurnell et al., 2012). In many regulated rivers, loss in lateral and vertical connectivity led to changes in species assemblages (Breton et al., 2023; Janssen et al., 2021), in plant health (Godfroy et al., 2023) and in the dynamic of riparian habitats (Comiti et al., 2011; Serlet et al., 2018). While riparian vegetation can provide ecosystem services that benefit biodiversity and human activities (Riis et al., 2020), the development of vegetation in river corridors can also lead to changes in roughness, facilitating fine sediment deposition that increase flooding risk, notably in embanked reaches (Vargas-Luna et al., 2015). In such a context, managing riparian vegetation through rejuvenation operations is required. These operations comprise vegetation clearing and bar reprofiling, by lowering topographic levels and exporting fine sediments. While such operations can benefit pioneer riparian plants communities (Janssen et al., 2023), questions remain about the sustainability of these operations and the habitats that have been recreated. This is especially true for highly-anthropized rivers where changes in flow and sediment regimes led to rapid vegetation recruitment and establishment (Comiti et al., 2011; Serlet et al., 2018).

Pioneer stages of riparian vegetation are shaped by hydrological and geomorphological drivers (Corenblit et al., 2014; Karrenberg et al., 2002; Mahoney and Rood, 1998; Stella et al., 2006). For example, flow pulses during the growing season have been shown to lead to seedling mortality and reduced survival for the *Salicaceae* (Carter Johnson, 2000; Dixon, 2003; Stokes, 2008). However, these drivers often interact at multiple spatial and temporal scales, and it remains challenging to understand their relative importance and threshold effects associated with them (but see Corenblit et al., 2024a; Pasquale et al., 2014; Stokes, 2008). This requires monitoring and assessing the trajectory of riparian

communities following rejuvenation operations over large spatial and temporal extend. Nevertheless, such high frequency monitoring, covering entire river reaches, has very rarely been possible using field-based approaches (González et al., 2015). Furthermore, although *ex situ* experiments have successfully identified the drivers influencing seed germination, such as air temperature and substrate moisture (Chen et al., 2013; Van Splunder et al., 1995), they cannot incorporate the effects of flow regime and geomorphic changes. Advances in remote sensing over the past decades are promising for high frequency monitoring of vegetation recruitment and establishment over large and continuous spatial extents (Corenblit et al., 2024b; Huylenbroeck et al., 2020; Piégay et al., 2020; Viles, 2016).

Components of riparian vegetation has been extracted from imagery for three decades now, using increasingly-advanced image processing techniques (Carbonneau et al., 2020; Dufour et al., 2012). Satellite time-series (*i.e.*, with a coarse spatial resolution but a dense temporal resolution) have been used to investigate the links between vegetation dynamics and hydrology. Combining field monitoring and Landsat data on the Yangtze River (China) for 20 years, Mei et al. (2025) demonstrated a rise in vegetation cover following reduced flow conditions and shortened submergence periods associated with active restoration efforts to promote vegetation development. On the Po River (Italy), Nones et al. (2024) also used Landsat data to show that the trend toward vegetation encroachment was linked to interactions between past human pressures and climate change, resulting in longer and more frequent dry periods. The role of floods in vegetation destruction was furthermore highlighted using ASTER satellite data on a reach of the Tagliamento River (Italy), where contrasting responses of riparian vegetation to flooding, based on differences in vegetation vigour, were highlighted (Bertoldi et al., 2011a). However, while satellite data provides critical insights on how vegetation responds to changes in flow regimes, they are limited by their low spatial resolution. This may induce a mismatch between the year of recruitment and a year of detection and can prevent a finer scale understanding of the ecological processes driving these trends from year to year.

At a finer spatial resolution, studies were conducted using aerial images from airplanes and drones. Time-series of historic aerial images were used to retrieve similar trends as satellite observations, for example with studies on vegetation development on the Isère River being able to go back to the 1930s (Serlet et al., 2018; Vautier et al., 2002). While the temporal depth of these datasets is appealing, their temporal resolution is often poor with gaps of multiple years between surveys. On the other hand, yearly surveys over smaller time-periods were able to shed light on the ecological and hydrological processes behind vegetation recruitment and establishment. On the Drome River (France), Räpple et al. (2017) used yearly aerial images to link recruitment with hydro-climatic drivers such as flow timing and intensity. Low flows and high temperatures following a reset of bare surfaces by floods were favourable to patch recruitment and expansion as there were no scouring floods both following seed dispersal and the winter. In addition, Maeda and Miyamoto (2025) used vegetation maps from UAV surveys acquired for 5 years on the Kinu River (Japan) to build a model predicting vegetation recruitment following a flood. They tested biological, hydrological and geomorphological predictors and showed that the presence of vegetation before the flood was one of the best predictors of vegetation recruitment, highlighting the role of biological processes related to resprout from plant fragments. However, there is still often a mismatch between the temporal and spatial resolution of the data used to monitor riparian vegetation and the ecological processes driving recruitment and establishment, as surveys using one image per year or less are very sensitive to acquisition timing.

Following multiple studies documenting rapid vegetation encroachment in the Isère River due to past and ongoing human pressures (Corenblit et al., 2020; Serlet et al., 2018; Vautier et al., 2002), the local stakeholders conducted rejuvenation operations over a 6 km reach, and acquired bi-yearly data to monitor vegetation response over a period of 7 years. The goal of this monitoring was to further our understanding of the processes behind vegetation development in the reach and to objectify when maintenance work is needed. This provides a unique framework to investigate the response of riparian vegetation to these actions and the hydrological drivers of vegetation dynamics in this reach. Therefore, in this paper, we (i) train a convoluted neural network to classify a bi-yearly time-series of

drone aerial images acquired over this reach, (ii) document the trajectory of vegetation patches (i.e., recruitment, lateral growth, destruction, resprouting) during six consecutive vegetative seasons following rejuvenation operations and (iii) test the effects of surface grain size, bar submersion and flooding on vegetation recruitment, establishment and destruction.

2. Study site.

The study was conducted on the Isère River, which is located in south-eastern France and is one of the main tributaries to the Rhône River (the mean annual flow at Grenoble is 178 $m3.s^{-1}$, the total length is 286 km and the catchment area is 11.890 km^2) [Figure 1]. The natural hydrological regime of the river was governed by snow and glacier melts with high flows from May to June (Vivian, 1969). The flow regime of the Isère River has been altered since the 1950s, increasing low flows during winter and reducing high flows during summer (Serlet et al., 2018; Vivian, 1994).

The floodplain of the river was strongly modified since the end of the 19^{th} century. The initial braided river was first channelized and artificially confined in an embanked channel along its entire length. Most of the floodplain has been converted into agricultural and urban areas. In the latter half of the 20^{th} century, sediments were intensively extracted in the main channel and the construction of dams and water bypasses modified the flow regime.

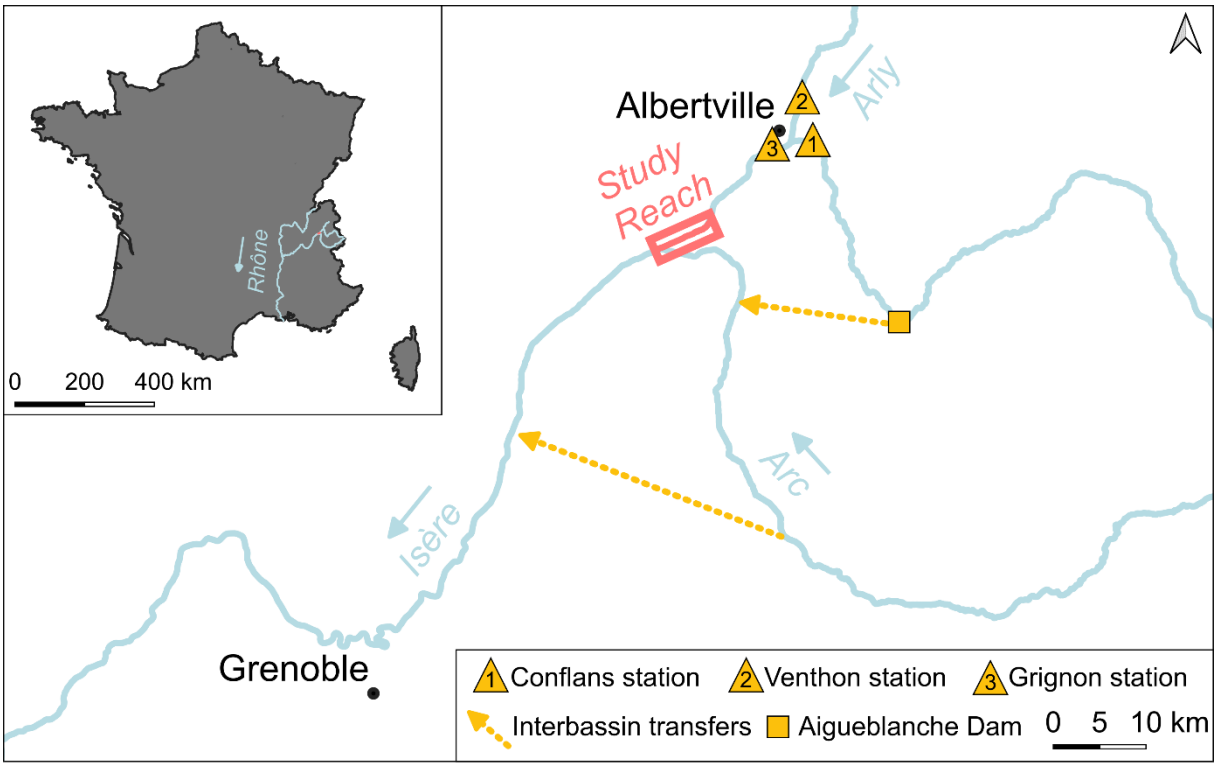

Figure 1. – Location of the study reach in France and on the Isère River.

Following channelization and until the 1950s, the fluvial style of the Isère River was characterized by alternate bare gravel bars. During high flow periods, those bars were eroded upstream and sediments were deposited downstream, leading to downstream bar migration that stopped plant succession at early pioneer stages (Didier, 1994). Geomorphic activity then progressively slowed following sediment extraction and damming, and vegetation encroachment and bar accretion was observed. Several studies were previously conducted to understand the drivers of vegetation encroachment. Vautier et al. (2002) noted an increase in the area of the vegetation in a reach of the Isère river from 5% in 1970 to 20% in 1996, which they attributed to changes in surface grain size and sediment transport. Serlet et al. (2018) analysed the timing of vegetation encroachment and the associated changes in bar morphology and mobility. They concluded that encroachment occurred following hydropower development and sediment mining in the studied reach and resulted in the formation of elongated and non-migrating bars. More recently, Corenblit et al. (2020) investigated the statistical relationship between vegetation successions and geomorphological variables at the bar level such as bar planform,

bar topography and fine sediment depth, obtained using time-series aerial images coupled with a field survey.

Our study covers a reach of about 6 km located in the Combe de Savoie, between the Grésy bridge and the confluence of the Isère and Arc rivers [Figure 1]. In this reach, the local river manager (SISARC) has carried out massive vegetation clearing and sediment removal operations to mitigate flood risk and recreate pioneer environments. Specifically, the reach was rejuvenated by removing woody vegetation and fine sediments from the bars and reshaping them to an elevation that favours frequent submersion. The rejuvenation work was conducted in three phases: (i) in the downstream portion of the study site in 2017, (ii) the upstream portion of the study site in 2018 and (iii) on two vegetated bars that had not yet been rejuvenated in winter 2021–2022 [Appendix F1A]. Since then, maintenance work (i.e., removal of vegetation and reshaping of bars without exporting fine sediments) has been carried out on two bars downstream the study reach in April 2021 [Appendix F1B] and on the bar located at the Grésy bridge in winter 2021–2022 [Appendix F1C].

3. Materials & Methods.

3.1. Remote sensing surveys and hydrological data.

Aerial visible images were acquired over the study reach each year between 2018 and 2023 by local stakeholders in order to investigate the processes behind vegetation development in the reach and to objectify when maintenance work is needed. For each year, two surveys were mobilized: one close to the beginning and one close to the end of the vegetation period [Appendix T1]. For each survey, a DJI Phantom 4 drone was flown at $\simeq$ 95 meters height over the active channel and sampled light in three spectral bands: red, green and blue. After the flight, all images were processed by the stakeholders using Agisoft Metashape in order to create an orthomosaic of the study site. The planimetric accuracy of the images was assessed both visually and using 46 permanent ground control points located near the roads on the embankments. We used these post-processed images for the analysis.

Hydrological data was retrieved using three different gauging stations upstream the study reach (data available at https://hydro.eaufrance.fr/). Due to multiple gaps in data availability, two different time series were created: 1) the data from the Grignon station on the Isère River 14 km upstream the study reach was extracted for the 2021–2023 period; 2) the data from the Conflans station on the Isère River and from the Venthon station on the Arly River were used to reconstruct a hydrological series for the 2018–2023 period. The data from each of these stations was aggregated on an hourly timestep and the daily mean discharge was calculated. The hygrogram for the aggregated time-series, along with the dates of all aerial images is presented on Appendix F2.

3.2. Image classification.

Images were first classified using a simple convolutional neural network (CNN) with seven hidden layers with ReLu as the activation function and of descending spatial size, and a final fully-convolutional layer used to predict the classes.

A training dataset was built by manually digitizing 125 regions of interest (ROI) for five classes (i.e., 25 per class) on each image: vegetation, fine sediments, coarse sediments, water and shadows. All classes were identified visually using photo-interpretation. Training and validation points were randomly sampled in each ROI with an 80-20 split using the *st_sample* function of the sf package for the R processing software (Pebesma, 2018; R Core Team, 2023) to obtain 10 000 training points and 2 500 validation points per image. Images were normalized and 16x16 training and validation patches were extracted using the Orfeo Toolbox meets TensorFlow (OTBTF) module built on Orfeo Toolbox and TensorFlow (Cresson, 2019). Patches from each image were combined to create a single training dataset for all images (totalling 120 000 training patches and 30 000 validation patches) and were used to train and validate a single neural network.

To further assess the accuracy of the two sediment classes, we used field measurements that were acquired as a part of the monitoring plan implemented by the stakeholders. Five surveys spanning multiple days were conducted between 2021 and 2023 but were not synchronous with the flights. For

each date, the sand-silt cover of six bars was surveyed by using a 5x5 meters grid and a visual assessment of the relative proportion of fine sediments (*i.e*., sands and silts) deposited above gravel in a 50 cm radius around each point of the grid (*i.e*., between 2273 and 2845 points per date). The relative proportion of fines was assessed using six discrete classes: 0–5%, 5–25%, 25–50%, 50–75%, 75–95% and 95–100%. For each of these points, the relative proportion of the fine sediments class compared to the coarse sediments class (*i.e.*, not counting surfaces that were classified as shadows or vegetation) was calculated in the 50 cm radius using the closest image available. The relative proportion of fine sediments from the classified images and from the in-field surveys were then compared for each field–image couple.

3.3. Patch extraction and semantic classification of change.

To create change maps between each date, the vegetation class was vectorized and gravel bars were manually digitized at low flow conditions each year (i.e., at the end of summer). This layer was used as a mask to remove the vegetation on the riverbanks, that overhangs above the active channel, and the biofilm cover which develops in side channels and shallow water areas. Vegetation patches were then extracted by keeping all polygons with an area > 2 meters (Räpple et al. 2017) and trends in vegetation cover at the pixel level and at the patch level were compared.

Spatial operations were used on vegetation patches to provide insights on vegetation changes. Intersections and differences across layers from the most recent to the oldest were used to extract the previous geometry of each vegetation patches and assign changes to four states:

(a) Recruitment: defined as the appearance of a vegetation patch that did not intersect a vegetation patch at the end of the previous vegetative season;

(b) Lateral growth: defined as the difference between the spatial extent of a vegetation patch at the end of the current vegetative season and the spatial extent of all patches it intersects (n > 1) from the end of the previous vegetative season;

(c) Resprouting and annual plants: defined as vegetation that was already present at the end of the previous vegetative season but not at the beginning of the current vegetative season;

(d) Removal: defined as vegetation that was present at the end of the previous vegetative season but is not present anymore at the end of the current vegetative season;

3.4. Analysis framework.

Vegetation dynamics were assessed at the reach scale. For each year, the surface area corresponding to each vegetation state was calculated in order to assess trends in vegetation cover. To control for the effects of changes in hydrology and overbank fine sediments cover across dates, the area of the digitized gravel bars and the proportion of both vegetation and fine sediments on the bars were also extracted for each year. In addition, vegetation dynamics were further assessed by exploring the longitudinal vegetation encroachment pattern using a spatially-continuous segmentation of the river reach into successive discrete river segments of 100 m long (Alber and Piégay, 2011). This process was achieved using the segmentation algorithm of the Fluvial Corridor Toolbox (see Rousson and Dunesme, 2024; Roux et al., 2015).

Three variables were then investigated as potential drivers: the initial state of new vegetation pixels, the time since the last rejuvenation operation and hydrology.

To identify the initial state of each vegetation pixels (i.e., the class at the beginning of the season), change rasters were produced for each vegetation season. Each time, the vegetation layer was reclassified using the change states to obtain initial information for each state. The difference in bar geometry between dates due to the higher flows at the beginning of the season was accounted for by

reclassifying as “water” all pixels that were in the spatial extent of the bar at the end of the season but not at the beginning.

To understand the effects of rejuvenation operations on vegetation encroachment, the relative area of vegetation on the bars was assessed each year depending on the time since the last operation. Intersection and difference operations between years were used to obtain a map of surface age from the last clearing operation.

To link hydrology and vegetation recruitment, we calculated the number of days during the seed dispersal period for which the daily mean discharge exceeded different ecological thresholds. We started with an initial threshold of 125 $m^3.s^{-1}$ that had been previously identified by Jourdain (2017) as the (critical) discharge for which bar coarse sediments was entrained on sparsely-vegetated bars before the rejuvenation work was conducted in the reach. We iterated on this initial threshold with a 10 $m^3.s^{-1}$ step and across a range of ± 30 $m^3.s^{-1}$ and determined the coefficient of determination of the relationship between the area of recruited patches and the number of days the threshold was exceeded. Based on field observations, the May–June period was selected for the recruitment of the Salicaceae species present in the study site.

To link hydrology and vegetation destruction, the values of the “Removal” vegetation class were first adjusted by removing polygons that were overlapping with the spatial extent of rejuvenation and maintenance operations in the reach. For each hydrological period (P_i) corresponding to an observation of vegetation destruction (*i.e.*, between two end-of-summer acquisitions), we calculated the excess flow power of flood peaks (Arnaud et al., 2017; Bagnold, 1966). For this, we selected a critical discharge value of 200 $m^3.s^{-1}$ based on the current discharge range targeted by stakeholders for dam flushing and releases (200–250 $m^3.s^{-1}$) and whose current aim is to promote erosion and sedimentation processes in the reach. We also summed the number of hours where Qmean ≥ 200 $m^3.s^{-1}$ for each hydrological period. Two variables were calculated for the excess flow power:

- (i) The excess flow power per unit area ($\omega_{max} - \omega_{200}$, in W.m^{-2}) defined as $\frac{\rho g(Q_{max} - Q_{200})S}{w}$, where ρ is the water density equal to 1000 kg.m^{-3}, g is the acceleration due to gravity equal to 9.81 m.s^{-2}, Q_{max} is the maximum hourly discharge within P_i, Q_{200} is the discharge equal to 200 m^3.s^{-1}, S is the channel slope of the reach equal to 0.0019 m.m^{-1}, and w is the median active channel width equal to 95 m;

- (ii) The sum of the unit excess flow power for flood peaks ($\sum^{P_i}(\omega_{max} - \omega_{200})$, in W.m^{-2}) defined as $\sum^{P_i} \frac{\rho g(Q_f - Q_{200})S}{w}$, where Q_f are the hourly peak discharges of each event summed within P_i.

4. Results.

4.1. Classification accuracy.

A single classifier was trained to process all images in the time-series and reached an overall accuracy of 0.97 and a kappa index of 0.97 on the validation data. The confusion matrix [Appendix T2] suggests that confusion between classes occurs mainly between the fine sediments class and either the coarse sediments class or the water class. Visual inspection of the classified images shows the limitations of the trained classifier, which is sensitive to changes in the properties of the water column [see Appendix F3 for details].

Comparison of the fine sediments class with in-field observations shows that the proportion of fine sediments on bar surfaces tends to be underpredicted by classifier [Appendix F4]. For two of the five surveys (A and C), a 75–95% cover in the field was estimated at around 50%, while it was estimated at around 75% for the three other surveys (B, D, E). On average, when fine sediments cover was lower than 50% in the field, the proportion of pixels classified as fine sediments was lower than 10%. Therefore, pixels classified as fine sediments are mostly coherent with in-field observation of surfaces dominated by fine sediments and not with coarser materials or a mix of fine and coarse material.

298

299 *4.2. Riparian vegetation dynamics at the reach scale.*

300 Vegetation cover was initially low following the two years of clearing operations and started to increase
301 in 2019 [Figure 2a]. Maintenance work during winter 2020–2021 and winter 2021–2022 led to a
302 reduction in vegetation cover but the system recovered to pre-maintenance state in a two-year
303 timeframe. During the study period, vegetation cover increased by a factor of five, reaching its highest
304 value at the end of summer 2023.

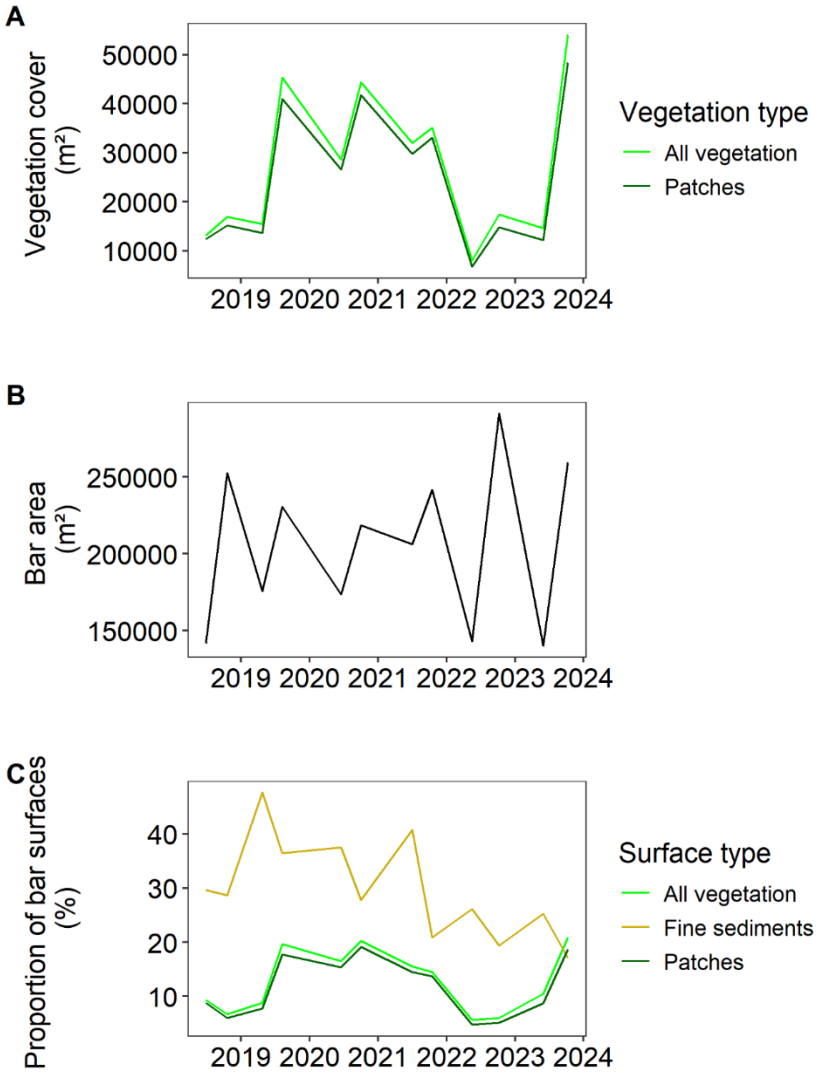

305 **Figure 2.** – Evolution of A) vegetation cover in the study site for all pixels classified as vegetation on
306 the bars and for vegetation patches, B) bar surface area (i.e., bare and vegetated) and C) the
307 proportion of bar surface area occupied by vegetation, vegetation patches or fine sediments.

The bi-yearly trends in vegetation cover are similar between all pixels classified as vegetation and vegetation patches (i.e., area ≥ 2m). Each year, vegetation cover increases due to growth and recruitment during the vegetative period and decreases during the off-season, either due to the death of plant with an annual life cycle, destruction, submersion, burial, or a lack of detection at the beginning of the vegetative period.

At the same time, bar area varied seasonally with higher area (≃ 250 000 m² (± 10%)) at the end of vegetative periods, when the flow level is lower [Figure 2b]. It was highest following rejuvenation and maintenance operations in 2022. Overall, vegetation encroachment covered 15% to 20% of bar surfaces starting from the end of the 2019 vegetative season to the maintenance operations that cleared vegetation on targeted bars [Figure 2c]. Those operations resulted in a drop of encroachment to around 5% but it rose again to 20% of bar surfaces at the end of summer 2023.

Fine sediments surfaces covered between 20% and 40% of the total area of bars in the reach [Figure 2c]. Fine sediments cover was higher at the beginning of the vegetative season than at the end. They occupied around 35% of bar surfaces on average between 2018 and 2021 and dropped between 20% and 25% of bar surfaces starting the end of the 2021 vegetative season to the end of the survey period. Fine sediments cover reached a maximum of near 50% at the beginning of the 2019 vegetative season. Spatializing the distribution of vegetation encroachment along the study reach [Figure 3] shows a coherent increase in the proportion of vegetation on the bars for years where increases in overall vegetation cover occurred.

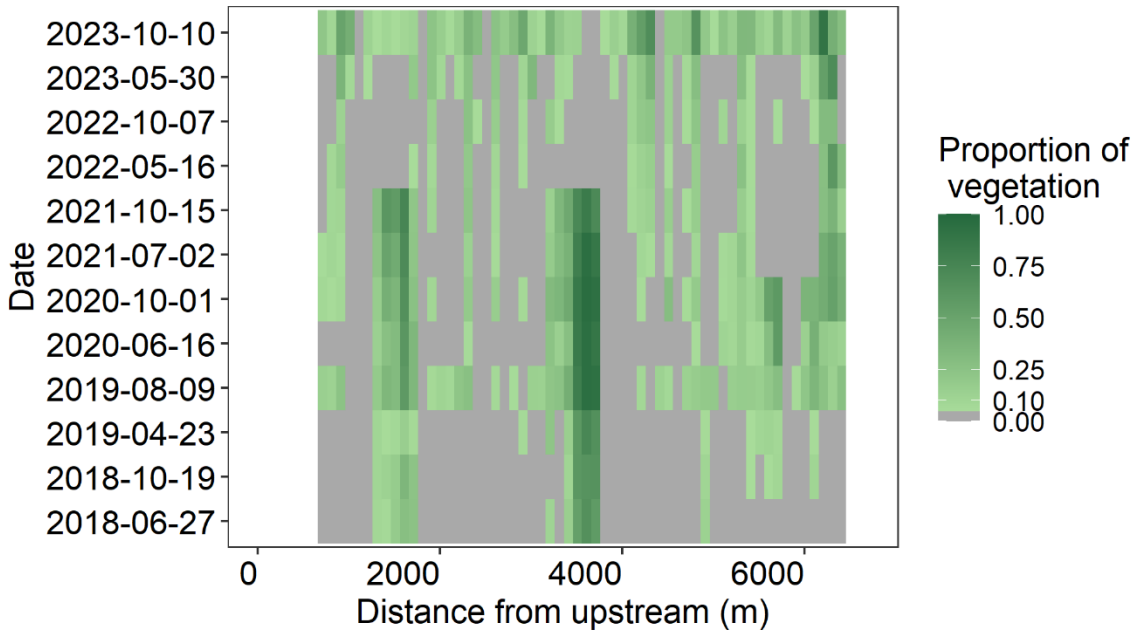

328 **Figure 3.** – Vegetation encroachment on bars along 100 meters segments. When the proportion of
329 vegetation on the bars in a DGO is between 0% and 5%, values are shown in dark grey instead.

330 At the beginning of the study period, vegetation was located on two vegetated bars that had not been
331 cleared during the initial rejuvenation work, and on an island downstream our study site [Figure 3].
332 Vegetation recruitment in 2018 occurred mainly in the downstream-most section – the first one to
333 undergo clearing work. Vegetation encroachment then increased on all gravel bars during summer
334 2019. The effects of targeted maintenance work to remove vegetation are visible near the confluence
335 in 2021 (near 5500 m in Figure 3) and on the two initially vegetated bars in 2022 (near 1500 m and
336 3500 m in Figure 3). At the end of the study period, most of the river reach is covered by vegetation,
337 with vegetation encroachment reaching more than 50% of the immerged bar surface in some of the
338 river segments.

339 The temporal resolution of the data allowed for the distinction of changes of vegetation into different
340 states [Figure 4]. Recruitment of new vegetation patches was the highest during 2023 and 2019. The
341 third highest year for patch recruitment was 2022, for which recruitment was still 2 to 3 times higher
342 than in 2018, 2020 and 2021. Patch growth was the highest in 2023 and 2019 and was also high the
343 years following high patch recruitment. The area from the lateral expansion of vegetation patches was

always higher than the one from appearing patches. The resprouting state reached a higher surface area than recruitment in 2020 and 2021. Partial or total destruction of vegetation patches was the highest during winter in 2019–2020, 2020–2021 and 2021–2022. The removal of vegetation due to maintenance work in 2021 and 2022 accounted for 75% and 91% of the loss in vegetation area respectively.

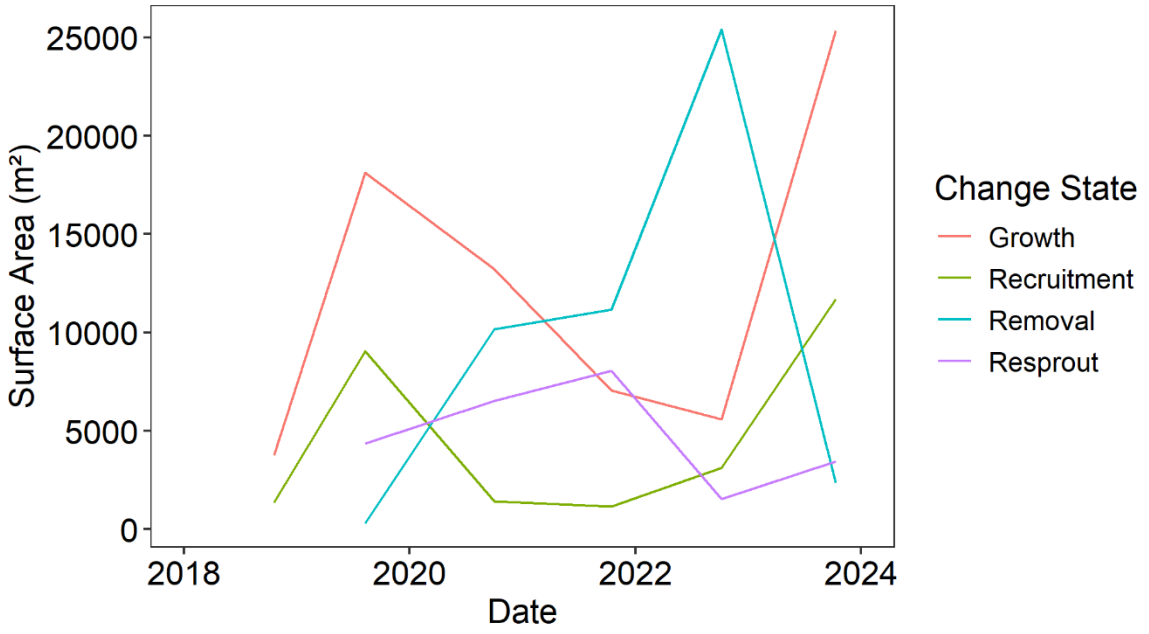

Figure 4. – Evolution of the surface area of all four different vegetation states each year in the study site: vegetation growth, vegetation recruitment, vegetation removal and vegetation resprout. The data shown is extracted from the spatial and temporal analysis of the vegetation patches.

4.3. Drivers of riparian vegetation recruitment, establishment and destruction.

The initial state of each pixel at the beginning of the vegetation period was investigated for all pixels identified as patch recruitment or patch growth [Table 1]. Although the total changes in vegetation area were different between years, recruitment was the highest (40%–60%) on the fine sediments class, with two exceptions: during the first and the last years of the study period. In 2018, recruitment occurred (73%) where sparse vegetation was already present at the end of June, whereas in 2023 recruitment mainly occurred (63%) in areas that were initially submerged. The trend was similar for patch growth, but with a lower relative proportion of pixels from the fine sediments class and a higher

relative proportion from sparse vegetation pixels (> 20% for all years besides 2023). Pixels classified as fine sediments were also the ones that became vegetated the most. Around 15% to 40% of fine sediments pixels in the spatial extent of the bars turned into vegetation at the end of the season, a higher value than for both the coarse sediments pixels and water pixels combined. Following the previously observed trends, inundated bar areas in spring 2023 were the ones that turned into vegetation the most. While up to 20% of vegetation was recruited on the coarse sediments class in 2022, less than 5% of the coarse sediments surfaces became vegetated at the end of summer. Recruitment on already vegetated pixels during spring occurred mostly in 2018, 2021 and 2022, years for which the first available image was later during the season: near the end of June.

		2018	**2019**	**2020**	**2021**	**2022**	**2023**
Recruitment from	*Fines*	1%	63%	58%	49%	58%	19%
	Coarse	0%	16%	9%	7%	22%	11%
	Vegetation	73%	5%	16%	38%	9%	6%
	Water	26%	15%	15%	5%	11%	63%
Growth from	*Fines*	1%	58%	48%	42%	53%	35%
	Coarse	0%	6%	5%	3%	12%	8%
	Vegetation	96%	21%	36%	47%	26%	15%
	Water	3%	14%	7%	3%	8%	38%
Fines to	*Vegetation patch*	0%	24%	17%	7%	15%	38%
	Sparse vegetation	0%	3%	2%	2%	3%	3%
Coarse to	*Vegetation patch*	0%	4%	2%	1%	2%	5%
	Sparse vegetation	0%	2%	1%	0%	1%	2%

Water to	*Vegetation patch*	0%	7%	4%	1%	1%	14%
	Sparse vegetation	1%	2%	2%	2%	1%	5%

Table 1. – Class transitions for each vegetative period: initial state of new vegetation from patch recruitment and patch growth, and proportion of the fine sediments, coarse sediments and water classes that becomes vegetation. Transitions from and into shadow are not shown.

The effect of time since the last rejuvenation operation revealed that encroachment was very low (< 2%) at the end of the summer following each operation [Figure 5]. It then increased to between 10% and 20% in a span of two to three years, with the timing of the increase corresponding to the years for which recruitment and lateral growth were the highest (*i.e.*, 2019 and 2023). For vegetation that was initially cleared in 2017, encroachment dropped in 2021 following maintenance operations in April, and for vegetation that was initially cleared in 2018, it dropped in 2022 following the maintenance operations during winter 2021–2022. At the end of the study period, encroachment was directly related to the time since last clearing, with older surfaces being more vegetated than newer surfaces.

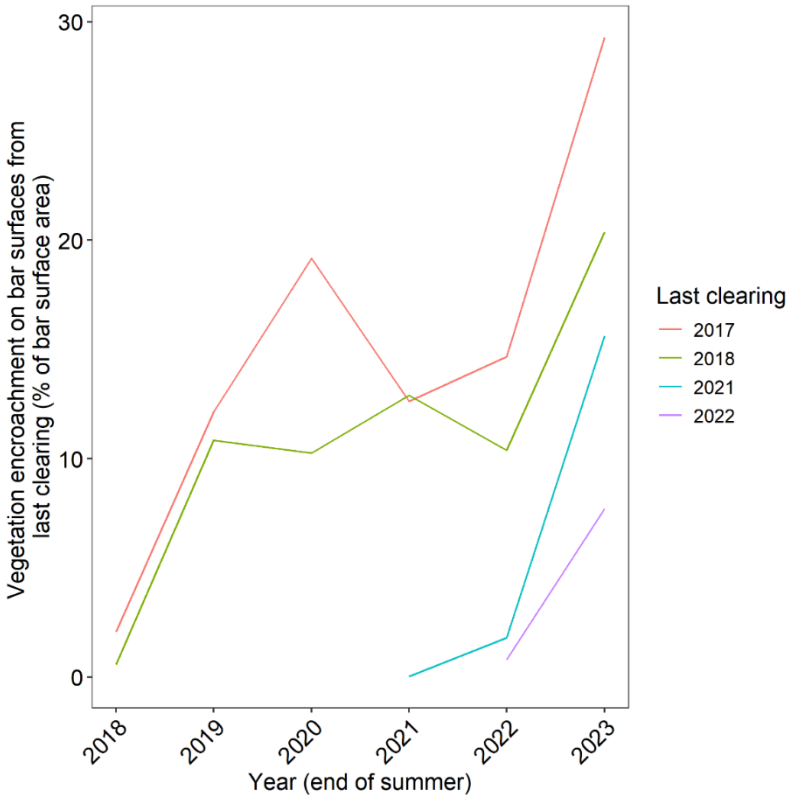

380 **Figure 5.** – Vegetation encroachment on bar surface area depending on the date of the last clearing
381 operation conducted. Changes in bar areas related to hydrology are excluded to keep only the
382 reworked surfaces.

383 Finally, the number of days hydrological thresholds were exceeded was plotted against the area of
384 recruited patches and the r^2 of the relationship reached its maxima at 0.76 for 125 $m^3.s^{-1}$ and 0.77 for
385 135 $m^3.s^{-1}$ [Figure 6A]. Although the number of observations was low, two distinct hydrological
386 conditions were observed during the vegetative period. The series of years for which patch recruitment
387 was the lowest (*i.e.*, 2018, 2020 and 2021) were also the ones for which the threshold of bar surface
388 mobility (*i.e.*, 125 $m^3.s^{-1}$) was exceeded for 30 days (*i.e.*, ≃50% of the time). On the other hands, the
389 years for which patch recruitment was the highest (*i.e.*, 2019, 2022 and 2023) were years for which
390 this threshold was exceeded for less than 7 days (*i.e.*, < 10 % of the time). The timing and duration of
391 events where the hourly discharge exceeded this lower threshold were mapped [Figure 6B], which
392 highlighted that events exceeding 125 $m^3.s^{-1}$ were spread out from the beginning of May to the end of
393 June during the years with low recruitment.

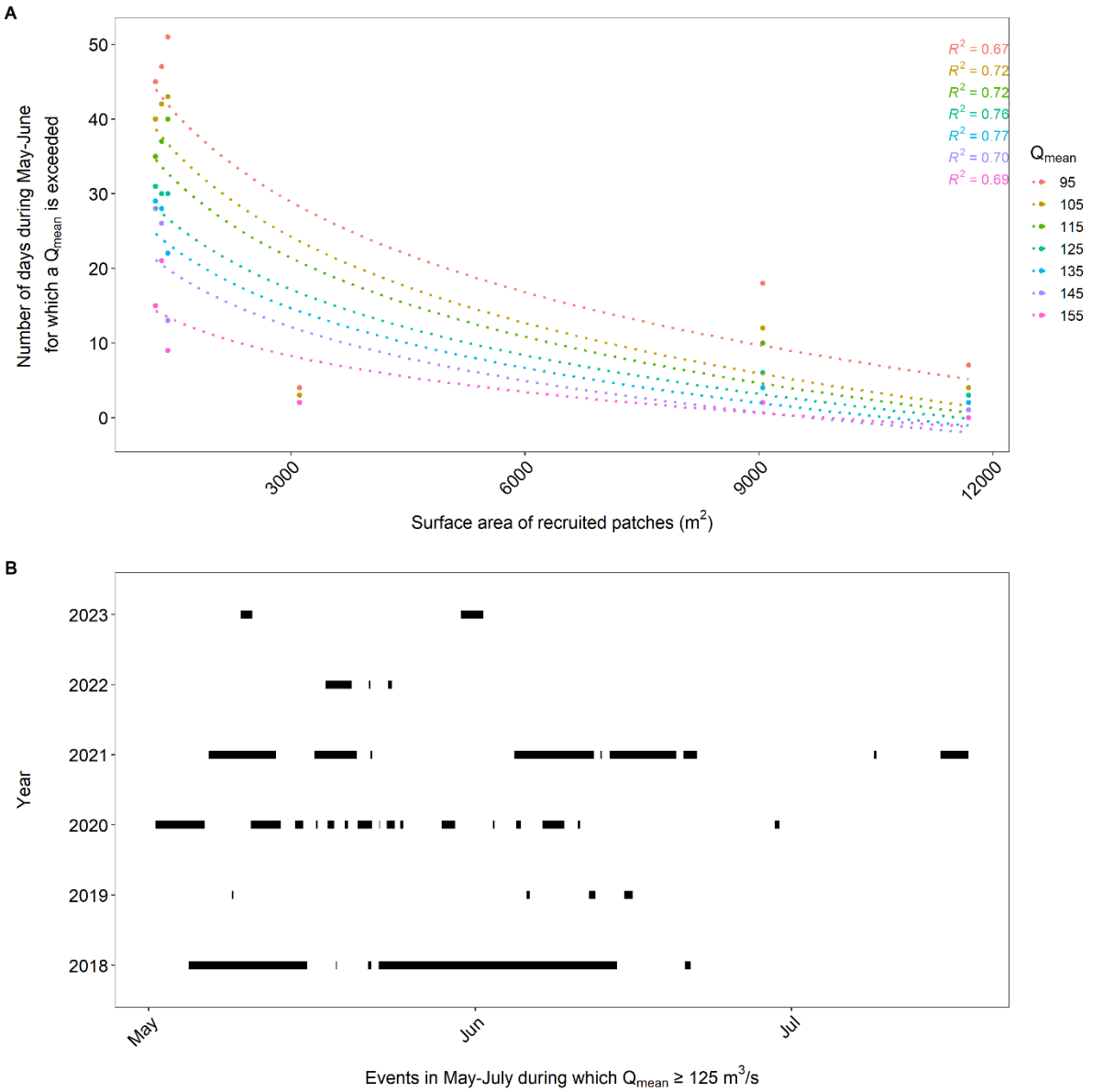

394 **Figure 6.** – A) Relationships between the number of days where different daily mean discharges
395 (Q_{mean}) are exceeded during the seed dispersion and germination period, and the surface area of
396 recruited patches for each year. B) Timing and duration of the events for which the hourly mean
397 discharge is equal to or exceeds 125 m^3/s^{-1}.

398 After removing the effects of rejuvenation operations, the area of vegetation that was destroyed each
399 year was the highest between 2019 and 2020, reaching 10 000 m^2 [Figure 7A]. This was also the period
400 for which the sum of the unit excess flow power for flood peaks was the highest [Figure 7B]. Although
401 it reached similar values between 2020 and 2021, this did not result in an increase in vegetation
402 destruction compared to other periods. Destruction was the lowest for the period immediately after

the rejuvenation work (*i.e.*, between 2018 and 2019), which was also the period for which excess flow power was the lowest.

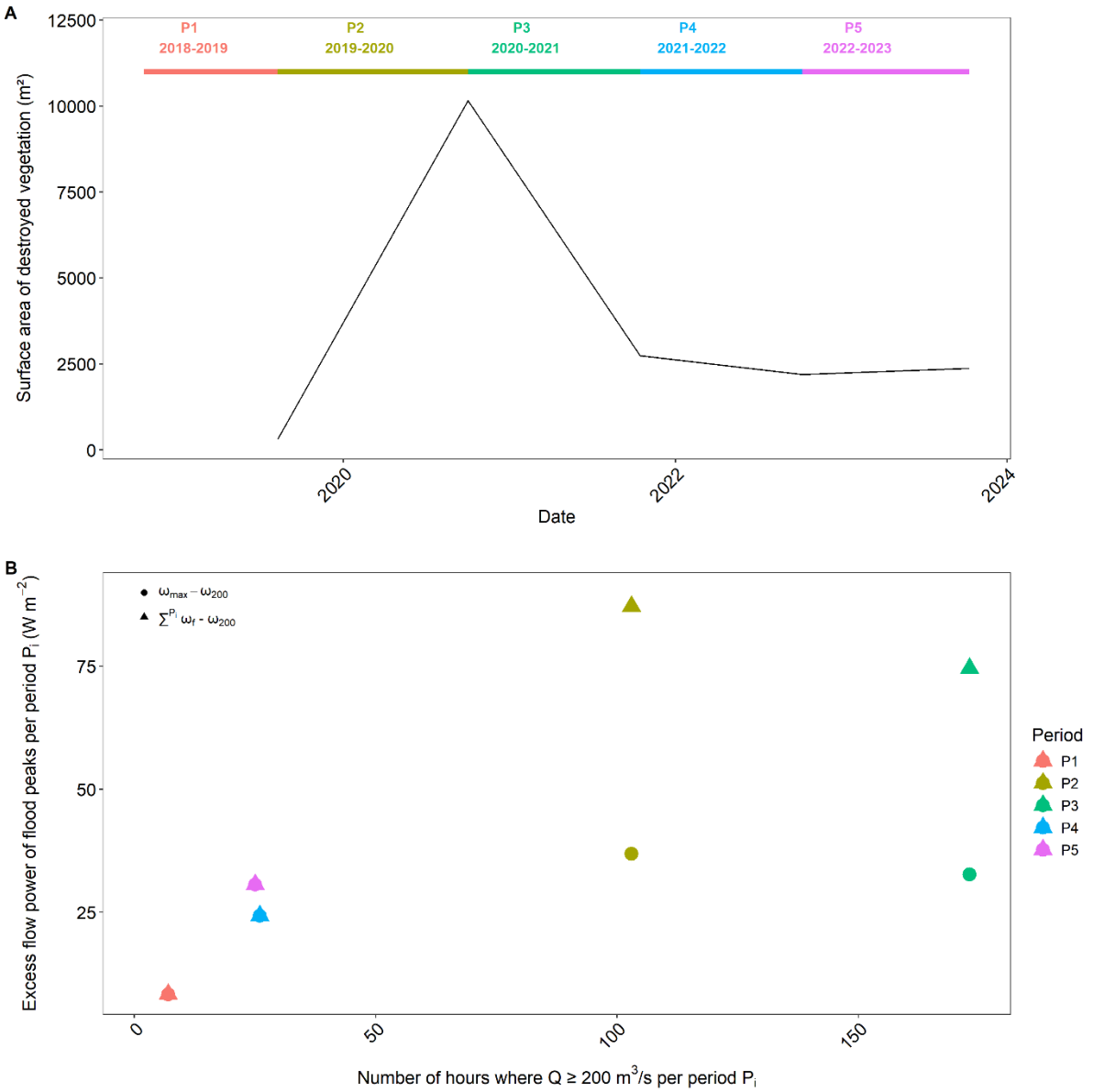

Figure 7. – A) Surface area of vegetation destroyed by the Isère River for each hydrological period P_i between two end-of-summer acquisitions. B) Relationship between the unit excess flow power metrics $\omega_{max} - \omega_{200}$, defined as $\frac{\rho g(Q_{max} - Q_{200})S}{w}$, and $\sum^{P_i}(\omega_{max} - \omega_{200})$, defined as $\sum^{P_i} \frac{\rho g(Q_f - Q_{200})S}{w}$, and the number of hours Q_{200} was exceeded for each hydrological period.

5. Discussion.

411 *5.1. Dynamics of riparian vegetation at the reach scale.*

412 Retrieving vegetation from the remote sensing data enabled us to investigate the dynamics of pioneer
413 vegetation on a 6 km reach of the Isère River. Vegetation encroachment fluctuated over time but a
414 general pattern of increasing cover was highlighted during the study period. Vegetation development
415 was rapid, reaching between 10% and 20% of bar surface from an un-vegetated state in a two-year
416 time frame following both the initial rejuvenation work and later maintenance actions. Although it
417 increased during the study period, vegetation encroachment was partly controlled by local
418 rejuvenation actions during the study period that reset ≃6 km of bar length, as vegetation
419 encroachment kept increasing on older surfaces.

420 Two distinct states were considered to understand increases in vegetation cover: lateral growth and
421 recruitment. Overall, our results highlighted that the increase in area from the lateral extension of
422 vegetation patches was higher than that from the recruitment of new vegetation patches. In this study,
423 lateral growth is determined through spatial operations that may be interpreted as different ecological
424 processes: the growth of individual plants, the creation of new stems through clonal development and
425 new seedling sprouting near established patches, as they create more favourable conditions for
426 seedlings recruitment (Corenblit et al., 2014; Politti et al., 2018). However, patch recruitment is still
427 necessary for patch growth, and large increases area attributed to patch growth followed increases
428 attributed to recruitment in the same year or the year before. These relationships between patch
429 expansion and recruitment are similar to the ones found on the Drome River (Räpple et al., 2017),
430 where the growth of established vegetation patches was also the main driver of encroachment
431 following an initial spike in recruitment after a reset by floods. We also investigated vegetation loss,
432 which was mainly driven by rejuvenation actions conducted by the stakeholders. Destruction of the
433 vegetation by the river flow was always lower than the combined increases in vegetation area from
434 lateral growth and recruitment. Finally, the intra-annual variability inside each vegetative season was
435 assessed using the resprout state, which included both resprout of vegetation buried by winter flows

altogether with annual plants that can quickly reach high biomass during one growing season. Resprout was initially higher than recruitment following the initial clearing work and the spike in recruitment during summer 2019 and then fell off when vegetation in the reach became older. This highlights the need to consider the intra-annual dynamics of riparian vegetation when surveying changes in vegetation cover, and that future studies would also benefit from the ability to better distinguish between woody pioneer vegetation and annual plants – for example using higher spectral resolution data that can enable species mapping (da Silva et al., 2022) or using higher temporal resolution to distinguish species by phenological differences (Michez et al., 2016).

5.2. Drivers of vegetation patterns

Hydrology played a key role in the recruitment and establishment of vegetation in the studied reach. Increases in vegetation encroachment during low-flow years occurred regardless of the time since the last clearing. Specifically, a window of at least two weeks of low-flow in May was observed the years where recruitment was the most important, while higher flows were consistent throughout the seed dispersal period when recruitment was low. However, amongst the three years for which high recruitment was observed (2019, 2022 and 2023), the driest year (2022) was also associated with the lowest area of recruited patches. As dry periods have been documented to lead to seedling mortality (Guilloy-Froget et al., 2002; Mahoney and Rood, 1998), we can hypothesize that survival rates could have been lower that year. Our overall observations about vegetation recruitment are coherent with the fact that flow pulses during the growing season are known to lead to seedling mortality for woody pioneer species (Carter Johnson, 2000; Dixon, 2003; Guilloy-Froget et al., 2002; Pasquale et al., 2014; Stokes, 2008) and with the observed response of green vegetation to dryer flows across multiple years (Cohen et al., 2022; Nones et al., 2024)**.** Applying a window of opportunity approach (Balke et al., 2011) to our observations is difficult because of the hydrological variability of the Isère River between years and because the end of the period where seed germination might occur each year is not clear and

might vary between species (Stella et al., 2006) and between years due to variations in temperatures (Bourgeois and González, 2019). Further research is therefore needed to characterize the seed dispersal period as well as work at a higher temporal resolution and with topographic data in order to better characterize submersion windows and the effects of specific flood events, but also to determine the relative contribution of annual and perennial species to patch recruitment and patch growth. Beside hydrology, we found that fine sediments deposits were more likely to become vegetated at the end of the season, both for patch recruitment and patch expansion. However, for lateral growth, these findings need to additionally consider the feedback between pioneer vegetation and sediments transport that facilitate sediments deposition (Corenblit et al., 2016). In years with higher flows when the initial state images were acquired, submerged areas were also likelier to become vegetated. This suggests that low flow areas where fine sediments are preferentially deposited and where moisture is high are the ones where vegetation establishes preferentially (Díaz-Alba et al., 2023; González et al., 2018).

The analysis of vegetation destruction shows that vegetation renewal from hydrological events was low during the study period. The floods that occurred during the period were comprised between two-year return time floods (Q2 = 290 $m^3.s^{-1}$) and five-year return time floods (Q5 = 415 $m^3.s^{-1}$) and the effect of floods with a higher instant discharge could not be assessed. The frequent floods that occur each year with a peak discharge of at least 200 $m^3.s^{-1}$ are not sufficient to induce a destruction of established patches. While there were two periods for which the sum of the excess flow power for flood peaks was high, only one of the them led to a peak in vegetation destruction (*i.e.*, the 2020-2021 period). From a hydrological standpoint, the main differences between 2019–2020 and the 2020–2021 hydrological periods were in the number of hours where the critical discharge was exceeded: it was higher during the 2020–2021 due to a higher number of smaller floods, while it was lower during 2019 – 2020 since two floods reached a peak discharge ≥ 350 $m^3.s^{-1}$. From an ecological standpoint, the state and the nature of riparian vegetation was also different during those two periods: the surfaces recruited spiked in summer 2019 and were far lower than the surfaces destroyed by the following

hydrological period (*i.e.*, 10 000 m²), while recruitment was low during summer 2020 and, as a result, surfaces recruited this year were lower than the surfaces destroyed by the following hydrological period (*i.e.*, 2500 m²). Our results suggest that vegetation that was able to establish and resist the floods from the 2019–2020 period was also able to resist the floods from the 2020–2021 period. An increasing resistance to flooding due to the rapid establishment of roots and the need for morphogenic change to uproot the plant for erosion has been shown in the literature for the perennial willows and poplars (Bywater-Reyes et al., 2015; Karrenberg et al., 2002; Politti et al., 2018), which contribute to the dynamics of vegetation patches in our study reach.

5.3. – Implications for river management and restoration.

González et al. (2015) considered active hydro-geomorphic actions such as water releases and bar levelling as parts of a larger panel of tools to restore riparian vegetation in rivers. The same measures can be also used to prevent vegetation encroachment, with studies citing both vegetation clearing (Janssen et al., 2023) and water releases (Loire et al., 2021; Rivaes et al., 2015) as potential tools to reset the system and remove established vegetation. In this study, we were able to assess the effects of vegetation clearing and of hydrological drivers on the dynamics of pioneer vegetation over a six years period.

On the Isère River, mechanical interventions on vegetated bars had a lasting impact on vegetation encroachment and forced a reset of the system. Before the rejuvenation operations, the vegetation cover in the reach was very high – reaching ≃70% of the total channel (Serlet et al., 2018). In 2023, vegetation cover occupied less than 30% of the surface of all bars that had been rejuvenated since the first clearing operations took place in 2017 which corresponds to ≃9% of the total channel. Targeted interventions on the more vegetated bars in 2021 and in 2022 had a local but visible effect on the repartition of vegetation at the reach scale but were still sensitive to recruitment and establishment during summer 2023. The nature of the vegetation was also different from before the rejuvenation

works as it was comprised of vegetation at the pioneer stage rather than the post-pioneer and mature upland forests that were described before (Corenblit et al., 2020).

Morphogenic flows in the Isère River currently target bar submersion and erosive processes using a range of discharges between 200 $m^3.s^{-1}$ and 250 $m^3.s^{-1}$ (Melun, 2024). Our results show that attempting to destroy established vegetation by erosion and uprooting would require the use of higher peak discharges (e.g., ≥ 350 $m^{3.}s^{-1}$) and would need to target the winter or spring following high vegetation recruitment, before it can establish further. While these values are not realistic for managing vegetation in the reach as attaining these discharges cannot be guaranteed, our results also show that promoting bar submersion can be effective to prevent the recruitment of vegetation. In particular, we identified a threshold between 125 $m^3.s^{-1}$ and 135 $m^3.s^{-1}$ that was inversely correlated to the area of recruited patches each year. These values are lower than the current flow level targets for morphogenic releases in the reach and could be tested to sustain submersion over a longer time period during the seed dispersal period. Therefore, while previous studies suggested that timing flow releases with the peak of the dispersal period was an active restoration method that could be implemented to promote the recruitment of Salicaceae (Mahoney and Rood, 1998; Rood et al., 2003), we suggest that flow releases following seed dispersal and germination can help prevent the development of vegetation in rivers where management needs are different.

6. Conclusion.

Bi-yearly colour aerial images acquired over a 6 km reach enabled the retrieval of both riparian vegetation and information on the surface grain size of gravel bars. The spatio-temporal dynamics of riparian vegetation were explored, showing a trend towards vegetation encroachment at the reach scale. The inter-annual variability of changes in vegetation cover was high and driven by patch recruitment and lateral expansion while vegetation destruction was mainly the result of targeted

536 rejuvenation actions. Encroachment was quick following rejuvenations actions and reached 20% of bar
537 surfaces in a two-year period.

538 Vegetation recruitment was found to be mainly driven by the hydrological conditions during the seed
539 dispersal and germination period. Flows between 125 $m^3.s^{-1}$ and 135 $m^3.s^{-1}$ were found to be correlated
540 with lower recruitment and are hypothesized to contribute to the mortality of young seedlings through
541 the submersion of the bars they generate. Under favourable hydrological conditions, vegetation
542 established on areas previously dominated by fine sediments or water, suggesting a preference for
543 areas of low elevation where fine sediments deposit and humidity is high. On the other hand, floods
544 were shown to have little impacts on vegetation in the reach: hydrological periods with high excess
545 flow power only led to vegetation destruction when vegetation had less than one year to establish.
546 This suggests that riparian vegetation in the Isère River establishes very quickly once seedlings survive
547 summer floods.

548 Our results have strong implications on the use of river flow in vegetation management. While current
549 practices suggest that eco-morphogenic flows could be used to limit vegetation encroachment in rivers
550 by destroying established vegetation, we suggest that sustaining summer flows could be used to limit
551 vegetation establishment.

552

553

554 **Acknowledgments.**

555 This work was cofunded by the French National Agency for Biodiversity (OFB) and INRAE. The remote
556 sensing data was acquired by Thibault Boissy (SISARC) as part of the “Plan de pérennisation de l’Isère
557 en Combe de Savoie” piloted by French institutions and stakeholders, i.e., Office Français de la
558 Biodiversité, Agence de l’Eau Rhône-Méditerranée-Corse, Direction régionale de l’environnement, de
559 l’aménagement et du logement Auvergne-Rhône-Alpes, Direction départementale des territoires de

Savoie, Electricité de France, Syndicat Mixte de l'Isère et de l'Arc en Combe de Savoie and Assemblée du Pays Tarentaise Vanoise.

Author contributions.

Julien Godfroy, Laurent Borgniet, Hervé Piégay, Gabriel Melun and Philippe Janssen conceived the ideas and designed methodology. Thibault Boissy collected the data. Julien Godfroy analysed the data. Julien Godfroy led the writing of the manuscript. All authors contributed critically to the draft and gave final approval for publication.

Data availability statement.

Raw data used in this study is the property of the stakeholders of the Isère River and is not made publicly available as it contains sensitive information outside the active channel. Post-processed data supporting the analysis, including masked and normalized aerial images over the active channel, classification results and the vegetation layers for each date, are available at https://doi.org/10.57745/USUGYX.

Conflict of interest statement.

The authors have no conflict of interest to declare.

Statement on inclusion.

Our study was conducted by scientists and stakeholders that were based in the country where the study was carried out. Both researchers and stakeholders at the national (Office Français de la Biodiversité) and local (Syndicat Mixte de l'Isère et de l'Arc en Combe de Savoie) level worked on the design of the study, and the data used was collected by the local stakeholders. They were associated to the writing of the paper and made critical contributions to the drafts. The results of this study were also conveyed more broadly to the other stakeholders involved in the integrative management of the Isère River basin (Plan de pérennisation de l'Isère en Combe de Savoie).

583 **Bibliography.**

584 Alber, A., Piégay, H., 2011. Spatial disaggregation and aggregation procedures for characterizing
585 fluvial features at the network-scale: Application to the Rhône basin (France).
586 Geomorphology 125, 343–360. https://doi.org/10.1016/j.geomorph.2010.09.009
587 Arnaud, F., Piégay, H., Béal, D., Collery, P., Vaudor, L., Rollet, A.-J., 2017. Monitoring gravel
588 augmentation in a large regulated river and implications for process-based restoration. Earth
589 Surface Processes and Landforms. https://doi.org/10.1002/esp.4161
590 Bagnold, R.A., 1966. An approach to the sediment transport problem from general physics (No. 422–
591 I), Professional Paper. U. S. Govt. Print. Off.,. https://doi.org/10.3133/pp422I
592 Balke, T., Bouma, T.J., Horstman, E.M., Webb, E.L., Erftemeijer, P.L.A., Herman, P.M.J., 2011.
593 Windows of opportunity: thresholds to mangrove seedling establishment on tidal flats.
594 Marine Ecology Progress Series 440, 1–9. https://doi.org/10.3354/meps09364
595 Belletti, B., Garcia de Leaniz, C., Jones, J., Bizzi, S., Börger, L., Segura, G., Castelletti, A., van de Bund,
596 W., Aarestrup, K., Barry, J., Belka, K., Berkhuysen, A., Birnie-Gauvin, K., Bussettini, M., Carolli,
597 M., Consuegra, S., Dopico, E., Feierfeil, T., Fernández, S., Fernandez Garrido, P., Garcia-
598 Vazquez, E., Garrido, S., Giannico, G., Gough, P., Jepsen, N., Jones, P.E., Kemp, P., Kerr, J.,
599 King, J., Łapińska, M., Lázaro, G., Lucas, M.C., Marcello, L., Martin, P., McGinnity, P.,
600 O'Hanley, J., Olivo del Amo, R., Parasiewicz, P., Pusch, M., Rincon, G., Rodriguez, C., Royte, J.,
601 Schneider, C.T., Tummers, J.S., Vallesi, S., Vowles, A., Verspoor, E., Wanningen, H., Wantzen,
602 K.M., Wildman, L., Zalewski, M., 2020. More than one million barriers fragment Europe's
603 rivers. Nature 588, 436–441. https://doi.org/10.1038/s41586-020-3005-2
604 Bourgeois, B., González, E., 2019. Pulses of seed release in riparian Salicaceae coincide with high
605 atmospheric temperature. River Research and Applications 35, 1590–1596.
606 https://doi.org/10.1002/rra.3505

607 Breton, V., Girel, J., Janssen, P., 2023. Long-term changes in the riparian vegetation of a large, highly
608 anthropized river: Towards less hygrophilous and more competitive communities. Ecological
609 Indicators 155, 111015. https://doi.org/10.1016/j.ecolind.2023.111015
610 Bywater-Reyes, S., Wilcox, A.C., Stella, J.C., Lightbody, A.F., 2015. Flow and scour constraints on
611 uprooting of pioneer woody seedlings. Water Resources Research 51, 9190–9206.
612 https://doi.org/10.1002/2014WR016641
613 Carbonneau, P.E., Dugdale, S.J., Breckon, T.P., Dietrich, J.T., Fonstad, M.A., Miyamoto, H., Woodget,
614 A.S., 2020. Adopting deep learning methods for airborne RGB fluvial scene classification.
615 Remote Sensing of Environment 251, 112107. https://doi.org/10.1016/j.rse.2020.112107
616 Carter Johnson, W., 2000. Tree recruitment and survival in rivers: influence of hydrological processes.
617 Hydrological Processes 14, 3051–3074. https://doi.org/10.1002/1099-
618 1085(200011/12)14:16/17%253C3051::AID-HYP134%253E3.0.CO;2-1
619 Chen, F.-Q., Wang, C.-H., Jia, G.-M., 2013. Ecology of *Salix variegata* seed germination: Implications
620 for species distribution and conservation in the Three Gorges region. South African Journal of
621 Botany 88, 243–246. https://doi.org/10.1016/j.sajb.2013.07.017
622 Cohen, T.J., Suesse, T., Reinfelds, I., Zhang, N., Fryirs, K., Chisholm, L., 2022. The re-greening of east
623 coast Australian rivers: An unprecedented riparian transformation. Science of The Total
624 Environment 810, 151309. https://doi.org/10.1016/j.scitotenv.2021.151309
625 Comiti, F., Da Canal, M., Surian, N., Mao, L., Picco, L., Lenzi, M.A., 2011. Channel adjustments and
626 vegetation cover dynamics in a large gravel bed river over the last 200years. Geomorphology
627 125, 147–159. https://doi.org/10.1016/j.geomorph.2010.09.011
628 Corenblit, D., Piégay, H., Arrignon, F., González-Sargas, E., Bonis, A., Davies, N.S., Ebengo, D.M.,
629 Garófano-Gómez, V., Gurnell, A.M., Henry, A.L., Hortobágyi, B., Martínez-Capel, F., Steiger, J.,
630 Tabacchi, E., Tooth, S., Vautier, F., Walcker, R., 2024a. Interactions between vegetation and
631 river morphodynamics. Part I: Research clarifications and challenges. Earth-Science Reviews
632 253, 104769. https://doi.org/10.1016/j.earscirev.2024.104769

633 Corenblit, D., Piégay, H., Arrignon, F., González-Sargas, E., Bonis, A., Ebengo, D.M., Garófano-Gómez,
634 V., Gurnell, A.M., Henry, A.L., Hortobágyi, B., Martínez-Capel, F., Mazal, L., Steiger, J.,
635 Tabacchi, E., Tooth, S., Vautier, F., Walcker, R., 2024b. Interactions between vegetation and
636 river morphodynamics. Part II: Why is a functional trait framework important? Earth-Science
637 Reviews 253, 104709. https://doi.org/10.1016/j.earscirev.2024.104709
638 Corenblit, D., Steiger, J., Charrier, G., Darrozes, J., Garófano-Gómez, V., Garreau, A., González, E.,
639 Gurnell, A.M., Hortobágyi, B., Julien, F., Lambs, L., Larrue, S., Otto, T., Roussel, E., Vautier, F.,
640 Voldoire, O., 2016. Populus nigra L. establishment and fluvial landform construction:
641 biogeomorphic dynamics within a channelized river. Earth Surface Processes and Landforms
642 41, 1276–1292. https://doi.org/10.1002/esp.3954
643 Corenblit, D., Steiger, J., González, E., Gurnell, A.M., Charrier, G., Darrozes, J., Dousseau, J., Julien, F.,
644 Lambs, L., Larrue, S., Roussel, E., Vautier, F., Voldoire, O., 2014. The biogeomorphological life
645 cycle of poplars during the fluvial biogeomorphological succession: a special focus on Populus
646 nigra L. Earth Surface Processes and Landforms 39, 546–563.
647 https://doi.org/10.1002/esp.3515
648 Corenblit, D., Tabacchi, E., Steiger, J., Gurnell, A.M., 2007. Reciprocal interactions and adjustments
649 between fluvial landforms and vegetation dynamics in river corridors: A review of
650 complementary approaches. Earth-Science Reviews 84, 56–86.
651 https://doi.org/10.1016/j.earscirev.2007.05.004
652 Corenblit, D., Vautier, F., González, E., Steiger, J., 2020. Formation and dynamics of vegetated fluvial
653 landforms follow the biogeomorphological succession model in a channelized river. Earth
654 Surface Processes and Landforms 45, 2020–2035. https://doi.org/10.1002/esp.4863
655 Cresson, R., 2019. A Framework for Remote Sensing Images Processing Using Deep Learning
656 Techniques. IEEE Geoscience and Remote Sensing Letters 16, 25–29.
657 https://doi.org/10.1109/LGRS.2018.2867949

da Silva, A.R., Demarchi, L., Sikorska, D., Sikorski, P., Archiciński, P., Jóźwiak, J., Chormański, J., 2022. Multi-source remote sensing recognition of plant communities at the reach scale of the Vistula River, Poland. Ecological Indicators 142, 109160. https://doi.org/10.1016/j.ecolind.2022.109160

Díaz-Alba, D., Henry, A.L., García de Jalón, D., González del Tánago, M., Martínez-Fernández, V., 2023. Salix regeneration in fluvial landscapes: Empirical findings based on a systematic review. Ecological Engineering 193, 107010. https://doi.org/10.1016/j.ecoleng.2023.107010

Didier, M., 1994. Relation entre l'enfoncement du lit de l'Isère et la stabilité de ses îles dans le Grésivaudan. Revue de Géographie Alpine 82, 147–155. https://doi.org/10.3406/rga.1994.3756

Dixon, M.D., 2003. Effects of flow pattern on riparian seedling recruitment on sandbars in the Wisconsin River, Wisconsin, USA. Wetlands 23, 125–139. https://doi.org/10.1672/0277-5212(2003)023%255B0125:EOFPOR%255D2.0.CO;2

Dufour, S., Muller, E., Straatsma, M., Corgne, S., 2012. Image Utilisation for the Study and Management of Riparian Vegetation: Overview and Applications, in: Fluvial Remote Sensing for Science and Management. John Wiley & Sons, Ltd, pp. 215–239. https://doi.org/10.1002/9781119940791.ch10

Entwistle, N.S., Heritage, G.L., Schofield, L.A., Williamson, R.J., 2019. Recent changes to floodplain character and functionality in England. CATENA 174, 490–498. https://doi.org/10.1016/j.catena.2018.11.018

Godfroy, J., Lejot, J., Demarchi, L., Bizzi, S., Michel, K., Piégay, H., 2023. Combining Hyperspectral, LiDAR, and Forestry Data to Characterize Riparian Forests along Age and Hydrological Gradients. Remote Sensing 15, 17. https://doi.org/10.3390/rs15010017

González, E., Martínez-Fernández, V., Shafroth, P.B., Sher, A.A., Henry, A.L., Garófano-Gómez, V., Corenblit, D., 2018. Regeneration of *Salicaceae* riparian forests in the Northern Hemisphere:

A new framework and management tool. Journal of Environmental Management 218, 374–387. https://doi.org/10.1016/j.jenvman.2018.04.069

González, E., Sher, A.A., Tabacchi, E., Masip, A., Poulin, M., 2015. Restoration of riparian vegetation: A global review of implementation and evaluation approaches in the international, peer-reviewed literature. Journal of Environmental Management 158, 85–94. https://doi.org/10.1016/j.jenvman.2015.04.033

Grill, G., Lehner, B., Thieme, M., Geenen, B., Tickner, D., Antonelli, F., Babu, S., Borrelli, P., Cheng, L., Crochetiere, H., Ehalt Macedo, H., Filgueiras, R., Goichot, M., Higgins, J., Hogan, Z., Lip, B., McClain, M.E., Meng, J., Mulligan, M., Nilsson, C., Olden, J.D., Opperman, J.J., Petry, P., Reidy Liermann, C., Sáenz, L., Salinas-Rodríguez, S., Schelle, P., Schmitt, R.J.P., Snider, J., Tan, F., Tockner, K., Valdujo, P.H., van Soesbergen, A., Zarfl, C., 2019. Mapping the world's free-flowing rivers. Nature 569, 215–221. https://doi.org/10.1038/s41586-019-1111-9

Guilloy-Froget, H., Muller, E., Barsoum, N., Hughes, F.M.M., 2002. Dispersal, germination, and survival of Populus nigra L. (Salicaceae) in changing hydrologic conditions. Wetlands 22, 478–488. https://doi.org/10.1672/0277-5212(2002)022%255B0478:DGASOP%255D2.0.CO;2

Gurnell, A.M., Bertoldi, W., Corenblit, D., 2012. Changing river channels: The roles of hydrological processes, plants and pioneer fluvial landforms in humid temperate, mixed load, gravel bed rivers. Earth-Science Reviews 111, 129–141. https://doi.org/10.1016/j.earscirev.2011.11.005

Huylenbroeck, L., Laslier, M., Dufour, S., Georges, B., Lejeune, P., Michez, A., 2020. Using Remote Sensing to charaterize riparian vegetation : a review of available tools and perspectives for managers.

Janssen, P., Chevalier, R., Chantereau, M., Dupré, R., Evette, A., Hémeray, D., Mårell, A., Martin, H., Rodrigues, S., Villar, M., Greulich, S., 2023. Can vegetation clearing operations and reprofiling of bars be considered as an ecological restoration measure? Lessons from a 10-year vegetation monitoring program (Loire River, France). Restoration Ecology 31, e13704. https://doi.org/10.1111/rec.13704

709 Janssen, P., Stella, J.C., Räpple, B., Gruel, C.-R., Seignemartin, G., Pont, B., Dufour, S., Piégay, H., 2021.
710 Long-term river management legacies strongly alter riparian forest attributes and constrain
711 restoration strategies along a large, multi-use river. Journal of Environmental Management
712 279, 111630. https://doi.org/10.1016/j.jenvman.2020.111630
713 Jourdain, C., 2017. Action des crues sur la dynamique sédimentaire et végétale dans un lit de rivière à
714 galets : l'Isère en Combe de Savoie (These de doctorat). Université Grenoble Alpes (ComUE).
715 Karrenberg, S., Edwards, P.J., Kollmann, J., 2002. The life history of Salicaceae living in the active zone
716 of floodplains. Freshwater Biology 47, 733–748. https://doi.org/10.1046/j.1365-
717 2427.2002.00894.x
718 Liébault, F., Piégay, H., 2002. Causes of 20th century channel narrowing in mountain and piedmont
719 rivers of southeastern France. Earth Surface Processes and Landforms 27, 425–444.
720 https://doi.org/10.1002/esp.328
721 Loire, R., Piégay, H., Malavoi, J.-R., Kondolf, G.M., Bêche, L.A., 2021. From flushing flows to
722 (eco)morphogenic releases: evolving terminology, practice, and integration into river
723 management. Earth-Science Reviews 213, 103475.
724 https://doi.org/10.1016/j.earscirev.2020.103475
725 Maeda, N., Miyamoto, H., 2025. A Logistic Regression Model for the Prediction of Vegetation
726 Recruitment in the Kinu River, Japan. River Research and Applications 41, 786–796.
727 https://doi.org/10.1002/rra.4418
728 Mahoney, J.M., Rood, S.B., 1998. Streamflow requirements for cottonwood seedling recruitment—
729 An integrative model. Wetlands 18, 634–645. https://doi.org/10.1007/BF03161678
730 Mei, J., Yang, Z., Yue, Y., Fan, Y., Liu, J., Li, M., Zhou, C., 2025. Timing Matters: Dual-Track Recovery of
731 Critical Habitats in Dam-Regulated Rivers. Environ. Sci. Technol.
732 https://doi.org/10.1021/acs.est.5c03783
733 Melun, G., 2024. Plan expérimental de pérennisation du lit de l'Isère en Combe de Savoie - Retour
734 d'expérience sur l'expérimentation de mai 2018. Office Français de la biodiversité.

735 Michez, A., Piégay, H., Lisein, J., Claessens, H., Lejeune, P., 2016. Classification of riparian forest
736 species and health condition using multi-temporal and hyperspatial imagery from unmanned
737 aerial system. Environmental Monitoring and Assessment 188, 19.
738 https://doi.org/10.1007/s10661-015-4996-2
739 Nones, M., Guerrero, M., Schippa, L., Cavalieri, I., 2024. Remote sensing assessment of
740 anthropogenic and climate variation effects on river channel morphology and vegetation:
741 Impact of dry periods on a European piedmont river. Earth Surface Processes and Landforms
742 49, 1632–1652. https://doi.org/10.1002/esp.5791
743 Pasquale, N., Perona, P., Francis, R., Burlando, P., 2014. Above-ground and below-ground Salix
744 dynamics in response to river processes. Hydrological Processes 28, 5189–5203.
745 https://doi.org/10.1002/hyp.9993
746 Pebesma, E., 2018. Simple Features for R: Standardized Support for Spatial Vector Data. The R
747 Journal 10, 439–446.
748 Piégay, H., Arnaud, F., Belletti, B., Bertrand, M., Bizzi, S., Carbonneau, P.E., Dufour, S., Liébault, F.,
749 Ruiz-Villanueva, V., Slater, L., 2020. Remotely sensed rivers in the Anthropocene: state of the
750 art and prospects. Earth Surface Processes and Landforms 45, 157–188.
751 https://doi.org/10.1002/esp.4787
752 Politti, E., Bertoldi, W., Gurnell, A., Henshaw, A., 2018. Feedbacks between the riparian Salicaceae
753 and hydrogeomorphic processes: A quantitative review. Earth-Science Reviews 176, 147–
754 165. https://doi.org/10.1016/j.earscirev.2017.07.018
755 R Core Team, 2023. R: A Language and Environment for Statistical Computing. R Foundation for
756 Statistical Computing, Vienna, Austria.
757 Räpple, B., Piégay, H., Stella, J.C., Mercier, D., 2017. What drives riparian vegetation encroachment in
758 braided river channels at patch to reach scales? Insights from annual airborne surveys
759 (Drôme River, SE France, 2005-2011). Ecohydrology 16. https://doi.org/10.1002/eco.1886

760 Riis, T., Kelly-Quinn, M., Aguiar, F.C., Manolaki, P., Bruno, D., Bejarano, M.D., Clerici, N., Fernandes,
761 M.R., Franco, J.C., Pettit, N., Portela, A.P., Tammeorg, O., Tammeorg, P., Rodríguez-González,
762 P.M., Dufour, S., 2020. Global Overview of Ecosystem Services Provided by Riparian
763 Vegetation. BioScience 70, 501–514. https://doi.org/10.1093/biosci/biaa041
764 Rivaes, R., Rodríguez-González, P.M., Albuquerque, A., Pinheiro, A.N., Egger, G., Ferreira, M.T., 2015.
765 Reducing river regulation effects on riparian vegetation using flushing flow regimes.
766 Ecological Engineering 81, 428–438. https://doi.org/10.1016/j.ecoleng.2015.04.059
767 Rood, S.B., Gourley, C.R., Ammon, E.M., Heki, L.G., Klotz, J.R., Morrison, M.L., Mosley, D.,
768 Scoppettone, G.G., Swanson, S., Wagner, P.L., 2003. Flows for floodplain forests: A successful
769 riparian restoration. BioScience 53, 647–656. https://doi.org/10.1641/0006-
770 3568(2003)053%255B0647:FFFFAS%255D2.0.CO;2
771 Rousson, C., Dunesme, S., 2024. Fluvial Corridor Toolbox - standalone Python application.
772 https://doi.org/10.5281/zenodo.14228638
773 Roux, C., Alber, A., Bertrand, M., Vaudor, L., Piégay, H., 2015. "FluvialCorridor": A new ArcGIS toolbox
774 package for multiscale riverscape exploration. Geomorphology, Geomorphology in the
775 Geocomputing Landscape: GIS, DEMs, Spatial Analysis and statistics 242, 29–37.
776 https://doi.org/10.1016/j.geomorph.2014.04.018
777 Serlet, A.J., Gurnell, A.M., Zolezzi, G., Wharton, G., Belleudy, P., Jourdain, C., 2018.
778 Biomorphodynamics of alternate bars in a channelized, regulated river: An integrated
779 historical and modelling analysis. Earth Surface Processes and Landforms 43, 1739–1756.
780 https://doi.org/10.1002/esp.4349
781 Stella, J.C., Battles, J.J., Orr, B.K., McBride, J.R., 2006. Synchrony of seed dispersal, hydrology and
782 local climate in a semi-arid river reach in California. Ecosystems 9, 1200–1214.
783 https://doi.org/10.1007/s10021-005-0138-y

784 Stokes, K.E., 2008. Exotic invasive black willow (Salix nigra) in Australia: influence of hydrological
785 regimes on population dynamics. Plant Ecol 197, 91–105. https://doi.org/10.1007/s11258-
786 007-9363-0
787 Surian, N., Rinaldi, M., 2003. Morphological response to river engineering and management in
788 alluvial channels in Italy. Geomorphology 50, 307–326. https://doi.org/10.1016/S0169-
789 555X(02)00219-2
790 Van Splunder, I., Coops, H., Voesenek, L. a. C.J., Blom, C.W.P.M., 1995. Establishment of alluvial forest
791 species in floodplains: the role of dispersal timing, germination characteristics and water
792 level fluctuations. Acta Botanica Neerlandica 44, 269–278. https://doi.org/10.1111/j.1438-
793 8677.1995.tb00785.x
794 Vargas-Luna, A., Crosato, A., Uijttewaal, W.S.J., 2015. Effects of vegetation on flow and sediment
795 transport: comparative analyses and validation of predicting models. Earth Surface Processes
796 and Landforms 40, 157–176. https://doi.org/10.1002/esp.3633
797 Vautier, F., Peiry, J., Girel, J., 2002. Développement végétal dans le lit endigué de l'Isère en amont de
798 Grenoble : du diagnostic à l'évaluation des pratiques de gestion. Revue d'Écologie (La Terre
799 et La Vie) 57, 65–79. https://doi.org/10.3406/revec.2002.6207
800 Viles, H., 2016. Technology and geomorphology: Are improvements in data collection techniques
801 transforming geomorphic science? Geomorphology 270, 121–133.
802 https://doi.org/10.1016/j.geomorph.2016.07.011
803 Vivian, H., 1994. L'hydrologie artificialisée de l'Isère en amont de Grenoble. Essai de quantification
804 des impacts des aménagements. Revue de Géographie Alpine 82, 97–112.
805 https://doi.org/10.3406/rga.1994.3753
806 Vivian, H., 1969. Les crues de l'Isère à Grenoble et l'aménagement actuel des digues. Revue de
807 Géographie Alpine 57, 53–84. https://doi.org/10.3406/rga.1969.3391
808

Supplementary Materials.

Appendix T1. – Characteristics of the datasets used in this study.

Date	Spatial resolution	Daily mean discharge	Days between flights
2018-06-27	5 cm	53 $m^3.s^{-1}$	115
2018-10-19	5 cm	15 $m^3.s^{-1}$	
2019-04-23	5 cm	59 $m^3.s^{-1}$	108
2019-08-09	5 cm	13 $m^3.s^{-1}$	
2020-06-16	5 cm	76 $m^3.s^{-1}$	107
2020-10-01	5 cm	43 $m^3.s^{-1}$	
2021-07-02	5 cm	54 $m^3.s^{-1}$	105
2021-10-15	5 cm	39 $m^3.s^{-1}$	
2022-05-16	5 cm	78 $m^3.s^{-1}$	144
2022-10-07	5 cm	17 $m^3.s^{-1}$	
2023-05-30	5 cm	112 $m^3.s^{-1}$	133
2023-10-10	5 cm	33 $m^3.s^{-1}$	

Appendix T2. – Confusion matrix of the classification on the validation data.

		Predicted class of the validation patches				
		Fine	**Coarse**	**Shadow**	**Vegetation**	**Water**
Actual class of the validation patches	**Fine**	5743	109	19	1	148
	Coarse	151	5788	0	1	40
	Shadow	26	0	5941	3	30
	Vegetation	3	2	1	5991	3
	Water	159	67	36	3	5735

Appendix T3. – Proportion of each surface class that became vegetation after the vegetative period. Both vegetation patches (≥ 2m²) and isolated (i.e., sparse) vegetation units (< 2 m²) are shown.

	Fine		**Coarse**		**Water**	
	Patches	*Sparse*	*Patches*	*Sparse*	*Patches*	*Sparse*
2018	0%	0%	0%	0%	0%	1%
2019	24%	3%	4%	2%	7%	2%
2020	17%	2%	2%	1%	4%	2%
2021	7%	2%	1%	0%	1%	2%
2022	15%	3%	2%	1%	1%	1%
2023	38%	3%	5%	2%	14%	5%

Appendix F1. – Before–after view of the bars that underwent (A) vegetation clearing work during winter 2021–2022, (B) maintenance work in April 2021 and (C) maintenance work during winter 2021–2022.

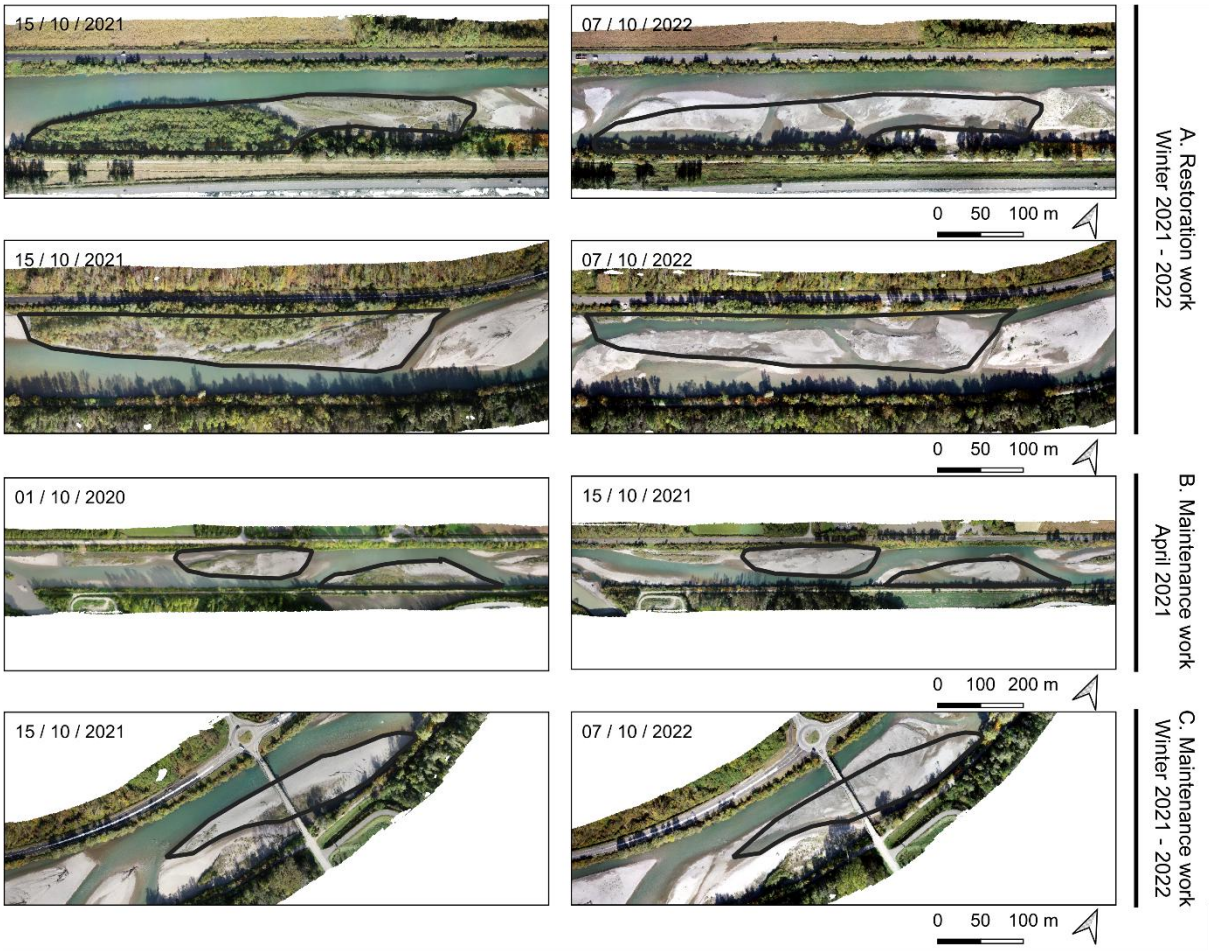

Appendix F2. – Daily mean discharge series merging the data from the Grignon station (from 2022) and the reconstructed series from the Conflans and Venthon stations (before 2022). The black dots are the date of acquisition for each aerial image and areas where the curve is interpolated are shown in light blue.

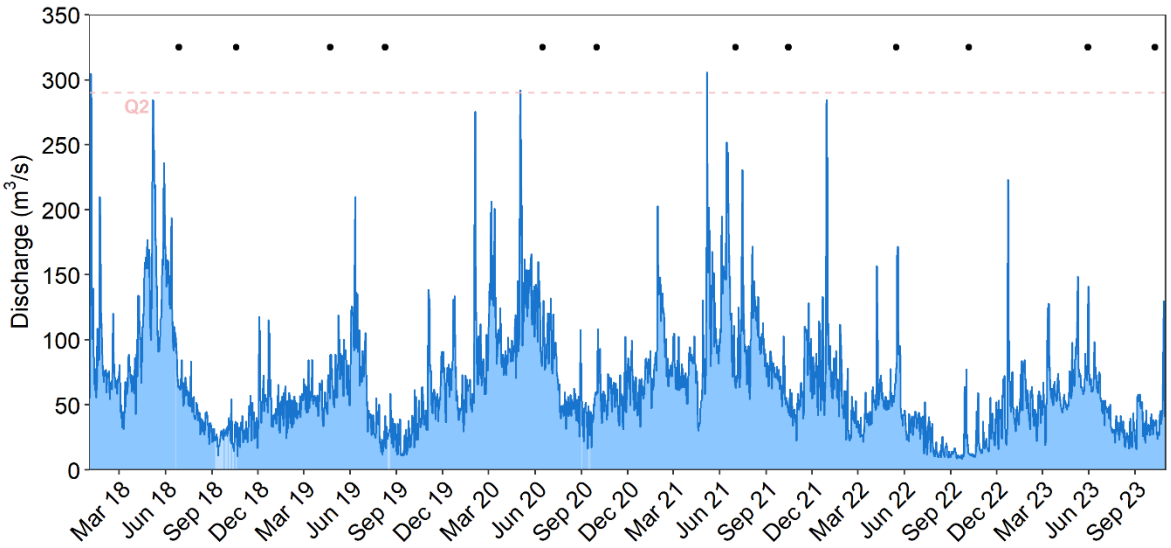

Appendix F3. – Panels highlighting the limitations of the trained classifier: (A) high turbidity, (B) low and transparent water table where submerged sediments are visible, (C) low water table on darker substrate and (D) biofilm cover.

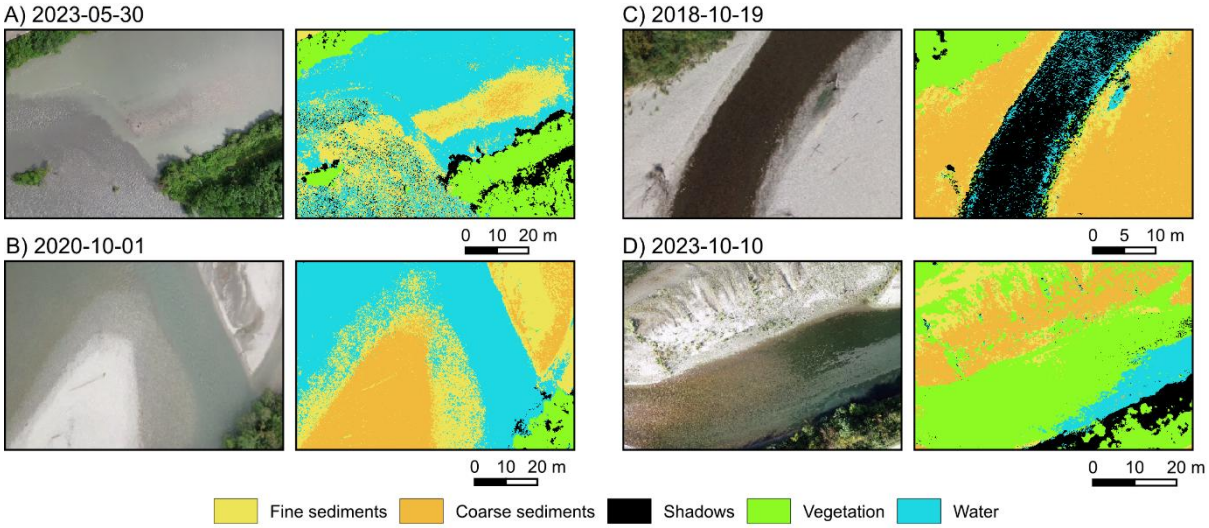

Appendix F4. – Comparison between the relative cover of fine sediments observed in field and predicted on the images.